Theoretical studies on optimum design of acousto-optic modulator using lithium niobate crystal

Zhaoguang Pang (庞兆广)*, Jie Li (李 洁), Yanlei Gao (高艳磊), and Zhenjun Yang (杨振军)

College of Physics Science and Information Engineering, Hebei Normal University, Shijiazhuang 050024, China

**Corresponding author: pangzhaoguang@163.com*

Received July 26, 2014; accepted October 28, 2014; posted online January 27, 2015

We theoretically study the optimum design of anisotropic acousto-optic modulator (AOM) based on lithium niobate crystal. Four different kinds of operating modes in the *XOZ* and *YOZ* acousto-optic (AO) planes are systematically analyzed by the tangent condition theory and the optimized operating mode is determined. Furthermore, the dependence of the AO merit on the operating frequency and the off-axis angle of the AOM are also obtained by numerical simulations.

OCIS codes: 160.1190, 170.1065, 230.1040, 230.4110.
doi: 10.3788/COL201513.S11601.

Acousto-optic modulator (AOM) is used to generate modulated diffracted laser beam by the refractive Bragg's diffraction of the acousto-optic (AO) crystal, which is widely applied in Q-switched laser[1–3], mode-locked fiber laser[4], optical tweezers[5], microscopy[6], acoustic velocity measurement[7], and sensors[8]. The bandwidth and diffractive efficiency are the two most important design parameters of the AOM, which are determined by the operating mode of the AOM. The AOM is commonly designed by the tangent momentum match condition[9,10], where the vector of the ultrasonic wave is designed tangent to the refractive index ellipsoid of the AO crystals to realize the broadband design of the AOM. However, in the previous study the diffractive efficiency properties of lithium niobate (LN) AOM under the momentum match condition have not been systematically carried out, which restricts the improvement of the properties of AOM based on the LN. In this letter, we systematically study the optimum design of AOM based on LN crystal, where the diffractive efficiency properties under four different kinds of AO interaction modes in the operating plane of the *XOZ* and *YOZ* planes are analyzed and the optimized operating mode is determined. The detailed features of the dependence of the AO merit on the operating frequency of the AOM are also obtained by numerical simulation.

The schematic diagram of LN anisotropic AO interaction under the tangent momentum match condition is shown in Fig. 1.

Note that the circular curves in Fig. 1 are the refractive index ellipsoids of the ordinary light and the ellipse curves are the refractive index ellipsoids of the extraordinary light, respectively. Here $\vec{k}_{\rm i}$,$\vec{k}_{\rm d}$, and $\vec{K}$ are the wave vectors of the incident light, the diffraction light, and the acoustic wave, $\theta_{\rm a}$ is named as the off-axis angle, which is between the vector of the ultrasonic wave and the *X*-axis; $\theta_{\rm i}$ is the incident angle which is between the vector of incident light and the *Z*–axis, and $\theta_{\rm d}$ is the diffractive angle which is between the vector of the diffractive light and the *Z*–axis. In order to realize the wideband design of the AOM, the $o \rightarrow e$ operating mode is selected for both ±order diffractions, thus the vector of the incident light is connected to the circular index curve (ordinary light) and the vector of the diffractive light is connected to the ellipse index curve (extraordinary light; Fig. 1). Furthermore, the vector of the ultrasonic wave is configured as tangent to the index ellipsoid of the extraordinary light for both the ±order diffractions, which contributes to realize the wideband design of the AOM.

Based on Figs. 1(a) and (b), the geometrical relationships of LN crystal under the tangent condition can be derived as

$$\theta_{\rm i}^{(1)} = \theta_{\rm a} - \cos^{-1}\left[\frac{n_{\rm d}}{n_{\rm o}} \cdot \cos\left(\theta_{\rm a} - \theta_{\rm d}\right)\right], \tag{1}$$

$$\theta_{\rm i}^{(2)} = 2\theta_{\rm a} - \theta_{\rm i}^{(1)}, \tag{2}$$

$$\theta_{\rm d} = \tan^{-1}\left(\frac{n_{\rm e}^2}{n_{\rm o}^2} \cdot \tan\theta_{\rm a}\right), \tag{3}$$

$$f_{\rm m}^{(i)} = \frac{v}{\lambda}\sqrt{n_{\rm o}^2 + n_{\rm d}^2 - 2n_{\rm o}n_{\rm d}\cos\left(\theta_{\rm d} - \theta_{\rm i}^{(i)}\right)}, \tag{4}$$

where $f_{\rm m}$ is the extreme frequency of the AOM, which is also defined as the central frequency of the AOM. The corner mark i means the order of the diffraction, where $i = 1$ means the +1 order diffraction and $i = -1$ means the −1 order diffraction.

The acoustic velocity in the *XOZ* and *YOZ* planes of LN crystal can be calculated by the Christoffel equation

$$\left(\Gamma_{ij} - \rho v^2 \delta_{ij}\right) \cdot u_j = 0, \tag{5}$$

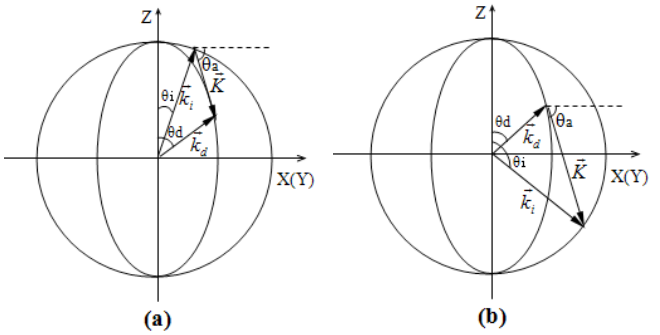

Fig. 1. Schematic diagram of the anisotropic AO interaction: (a) +1 order diffraction and (b) −1 order diffraction.

where $\Gamma_{ij} = L_{iJ}\, c_{JI}\, L_{Ij}$, ρ is the density of the crystal and v is the velocity of the ultrasonic. The ultrasonic velocity in the *XOZ* and *YOZ* planes can be obtained by solving the eigenvalue of Eq. (5), the reciprocal velocity curves are shown in Figs. 2(a) and (b).

Curve ① is named as the longitudinal wave and it can result in the isotropic AO interactions; curves ② and ③ are named as the fast sheared ultrasonic waves and slow sheared ultrasonic waves, which can lead to the anisotropic AO effect. In this letter, the four different sheared ultrasonic waves in the *XOZ* and *YOZ* planes are discussed for the optimum design of the AOM, respectively.

The diffraction efficiency of the AOM can be written as

$$\eta \approx \frac{\pi^2 M_2 L}{2\lambda^2 H} P_a, \tag{6}$$

where the parameter M_2 is the AO merit of the AOM, H and L are the height and length of the AO crystal, P_a is the power of the ultrasonic. From Eq. (6) it is easy to conclude the linearity relationship between the diffraction efficiency and the AO merit M_2, therefore the AOM designed with higher M_2 is required to improve the diffraction efficiency of the modulator. The expression of M_2 can be written as

$$M_2 = \frac{n_i^3 n_d^3 p_{\text{eff}}^2}{\rho v^3}, \tag{7}$$

where P_{eff} is the AO coefficient of the AO crystal.

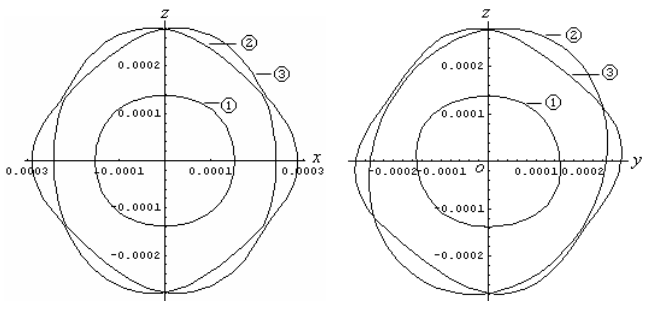

Fig. 2. Reciprocal velocity curves of LN crystal in (a) *XOZ* and (b) *YOZ* planes.

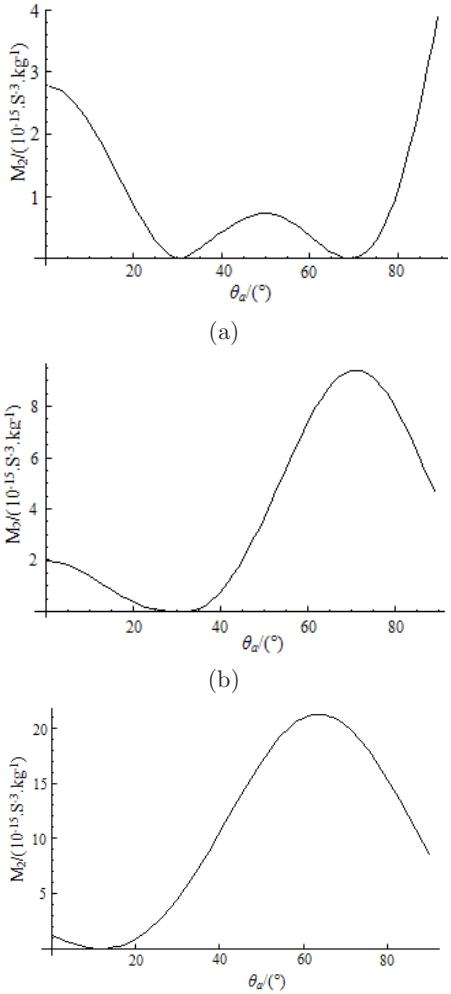

Fig. 3. Curves of M_2 versus θ_a under different operating conditions. Operating mode with the (a) fast sheared ultrasonic wave of *XOZ* plane, (b) slow sheared ultrasonic wave of *XOZ* plane, and (c) fast sheared ultrasonic wave of *YOZ* plane.

Based on Eqs. (1)–(7), the relationship between the parameters M_2 and θ_a under different operating modes can be calculated and the curves of $M_2(\theta_a)$~θ_a are shown in Figs. 3(a)–(c).

Different from the results illustrated in Figs. 3(a)–(c), the calculation results show that M_2 equals zero in the range of $\theta_a \in (0, \pi/2)$ under the operating mode of the fast sheared ultrasonic wave in the *YOZ* plane, which means that there is no AO effect under this operating mode. Thus, the optimum design of the AOM can be determined from the operating modes illustrated in Figs. 3(a)–(c).

Considering that the operating frequency of the AOM is usually designed at the order of 10^8 Hz, which means that the off-axis angle θ_a is set far less than 10°. Based on this deduction, it can be found that the operating mode with the fast sheared ultrasonic wave in the *XOZ* plane has the highest value of M_2, which can be determined as the optimum operating mode to obtain the higher performance of the AOM.

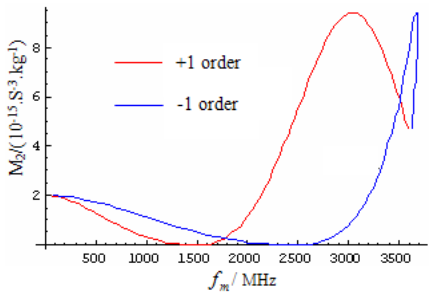

(a)

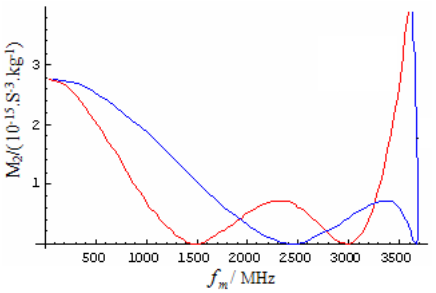

(b)

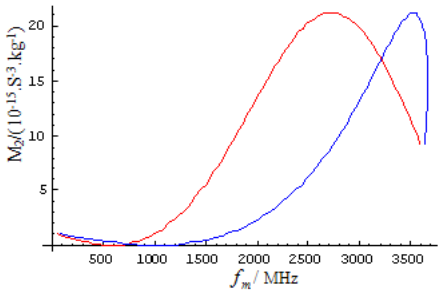

(c)

Fig. 4. Curves of M_2 versus f_m under different operating conditions: (a) curves of AO merit versus extreme frequency for slow ultrasonic wave in *XOZ* plane, (b) curves of AO merit versus extreme frequency for fast ultrasonic wave in *XOZ* plane, and (c) curves of AO merit versus extreme frequency for fast ultrasonic wave in *YOZ* plane.

For the convenience to design AOM with the parameter of central frequency, the relationships between M_2 and f_m have also been derived by numerical simulation, and the curves of $M_2 \sim f_m$ are shown in Figs. 4(a)–(c).

From Figs. 4(a)–(c), it can also be observed that the operating mode under the fast sheared ultrasonic wave in the *XOZ* plane achieves the highest value of M_2 under the condition of f_m<500 MHz. Furthermore, it can be observed that the operating mode with the −1 order diffraction achieves higher M_2 than that of the +1 order at a certain extreme frequency (Fig. 4(b)). Therefore, the optimum operating mode of the AOM can be determined as the operating mode of the −1 order diffraction with the fast sheared ultrasonic wave in the *XOZ* plane.

In conclusion, we carry out the optimum design of the LN AOM by the tangent momentum match condition. The properties of the AO merit are systematically calculated and the dependence of M_2 on the operating frequency and on the off-axis angle are both figured out by the numerical simulation and the optimum operating mode of the AOM is determined. This research work is useful for the improvement on the performance of the AOM and shows potential prospect in the applications of AO device.

This work was supported by the National Natural Science Foundation of China (Nos. 11374089 and 61308016), the Nature Science Foundation of Hebei Province (Nos. A2012205085, F2012205076, and A2012205023), and the Key Project of Hebei Education Department (No. ZD20131014).

References

1. T. W. Chen, K. C. Chang, and J. C. Chen, Appl. Opt. **53,** 3459 (2014).
2. M. Vallet, J. Barreaux, and M. Romanelli, Appl. Opt. **52,** 5402 (2013).
3. J. Kwiatkowski, J. K. Jabczynski, W. Zendzian, L. Gorajek, and M. Kaskow, Appl. Phys. B **114,** 395 (2014).
4. C. Cuadrado-Laborde, M. Bello-Jimenez, A. Diez, J. L. Cruz, and M. V. Andres, Opt. Lett. **39,** 68 (2014).
5. W. Benjamin Rogers and J. C. Crocker, Rev. Sci. Instrum. **85,** 043704 (2014).
6. S. P. Chong, C. H. Wong, K. F. Wong, C. J. R. Sheppard, and N. Chen, Biomed. Opt. Express **1,** 1026 (2010).
7. C. H. Lee and S. Hyuk, Opt. Express **22,** 13634 (2014).
8. T. H. Li, L. Huang, Y. T. Qiu, Q. Xue, and M. L. Gong, Opt. Eng. **52,** 034401 (2013).
9. Y. Y. Zhu, C. M. Zhang, and B. C. Zhao, Opt. Commun. **285,** 2332 (2012).
10. K. X. Yu, X. J. Shi, B. S. Zhao, and S. Y. He, J. Beijing Polytech. Univ. **28,** 211 (2002).